Equipping nanocarriers specifically toward cargo

Wieczorek, Sebastian; Remmler, Dario; Masini, Tiziana; Kochovski, Zdravko; Hirsch, Anna K H; Boerner, Hans G

Published in:
BIOCONJUGATE CHEMISTRY

DOI:
10.1021/acs.bioconjchem.6b00549

Publication date:
2017

Bioconjugate Chemistry

Article

pubs.acs.org/bc

Fine-tuning Nanocarriers Specifically toward Cargo: A Competitive Study on Solubilizing Related Photosensitizers for Photodynamic Therapy

Sebastian Wieczorek,[†] Dario Remmler,[†] Tiziana Masini,[‡] Zdravko Kochovski,[§] Anna K. H. Hirsch,[‡] and Hans G. Börner*[,†]

[†]Department of Chemistry, Laboratory for Organic Synthesis of Functional Systems, Humboldt-Universität zu Berlin, Brook-Taylor-Str. 2, 12489 Berlin, Germany

[‡]Stratingh Institute for Chemistry, University of Groningen, Nijenborgh 7, NL-9747 AG Groningen, The Netherlands

[§]Soft Matter and Functional Materials, Helmholtz-Zentrum Berlin für Materialien und Energie, Hahn-Meitner-Platz 1, Berlin, Germany

Supporting Information

ABSTRACT: Tailor-made drug solubilizers are studied based on peptide-poly(ethylene glycol) conjugates, which exhibit peptide segments constituting binding motifs for the small-molecule drugs of interest to render them water-soluble. Suitable 7mer peptides are selected via combinatorial means by screening large one-bead-one-compound (OBOC) peptide libraries. The capability of the screening method to read out structural detail of the drugs is investigated by comparing three related photosensitizers (Chlorin E6 (Ce6), Pheophorbide A (Pb*a*) and *meta*-tetra(hydroxyphenyl)chlorin (*m*-THPC), which are applicable for photodynamic cancer therapy. The screening procedure delivers de novo solubilizers that show the best solubilization efficiency for the drug the screening is performed with. While molecular recognition events between peptide and drug are not expected to be found, significant binding capacity differences of, e.g., the Ce6-solubilizer for Pb*a* are suggesting selectivity in drug binding, even among structurally closely related drugs. Cyro-Electron microscopy revealed the formation of colloidal aggregates between drug moieties and peptide conjugates. Insights into relevant amino acids in the identified peptide sequences are gained by studying capacities of systematic point mutations (alanine scans), enabling understanding of drug-binding motifs. These reveal the importance of sequence positioning of appropriate H-bonding between polar functional groups of the peptide and the drugs, which agrees well with computational binding studies performed on drug/peptide model complexes.

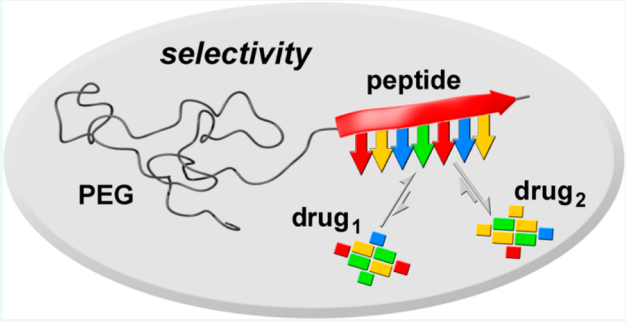

INTRODUCTION

Water insolubility of small-molecule drug compounds imposes one of the key limitations in pharmaceutical drug development.[1] Tremendous efforts are being spent to improve solubility and bioavailability of potential drug candidates to overcome undesired pharmaceutical profiles, which can otherwise cause adverse effects and eventually lead to structure failure.[2] Increasingly sophisticated drug formulation additives and drug delivery systems (DDS) are in development to not only improve drug bioavailability for therapeutic applications but also increase compound solubility to enable early drug structure testing without performing consecutive structure adaption cycles of a high-potential lead structures.[3−11] Still, the majority of DDS rely on unspecific, hydrophobic interactions of drug and carrier, e.g., in the case of amphiphilic block copolymer micelles, dendrimers, protein carriers, or liposomes.[12−18] Recently, biohybrid polymers composed of sequence-defined biosegments and synthetic polymers proved their potential for biomedical applications, enabling stealth or (bio)active coatings as well as responsive drug carriers or structured hydrogel scaffolds for tissue growth.[19−30] Beyond common strategies of established amphiphilic block copolymers, an approach has been described to more precisely adapt peptide-poly(ethylene glycol) (peptide-PEG) conjugates specifically to solubilize fluorescent or nonfluorescent drug entities.[31,32] Suitable peptides could be selected by screening large split&mix peptide libraries[33] for drug binding sequences. Besides experimental kinase inhibitors and anti-Alzheimer drugs, the fluorescence-based screening method was established for *meta*-tetra(hydroxyphenyl)chlorin (*m*-THPC, *Foscan*[34]) one of the most effective second generation chlorin-type sensitizers for photodynamic cancer therapy[35] (PDT).[8,31,32] Relevant

Special Issue: Peptide Conjugates for Biological Applications

Received: September 21, 2016
Revised: December 20, 2016
Published: December 21, 2016

DOI: 10.1021/acs.bioconjchem.6b00549
Bioconjugate Chem. 2017, 28, 760−767

parameters for drug carriers, like drug payload capacity, drug release kinetics, and aggregate shape could be fine-tuned by alteration of the peptide sequences, PEG-block length, and conjugate architecture.[31,36,37] The ability to trigger release was shown by introduction of reductively cleavable disulfide linkers into the peptide-based drug binding motifs.[38] Transient drug binding allows for the realization of "drug solubilizers", which appear to be advantageous for PDT. Tailored drug solubilizers sufficiently improve drug availability to enhance trans-solubilization kinetics of photosensitizers toward blood plasma proteins. These biological transport systems are exploited to ultimately distribute the photosensitizer systemically. Recent progress in the field of PDT benefits also from a structurally very rich and potent set of photosensitizers including chlorins, bacteriochlorins, and porphyrins.[39−42] The fundamental understanding of structure/mode-of-action relationships, with its underlying biophotophysics of types I and II reactive oxygen species production,[43] demands advanced drug formulation strategies. Even cellular compartment targeting of photosensitizers might become relevant to improve the clinically approved PDT.[44,45] However, other therapy forms will require stronger drug binding, resulting in effective drug hosting and transport in biosettings. To realize this, existing dermal delivery systems based on polymer nanogels could be equipped with peptide segments to specifically host *m*-THPC without jeopardizing the delivery activity through the skin barrier.[46]

Here, we elucidate the specificity of drug−peptide interactions in peptide-PEG conjugate-based solubilizers, which exhibit peptide sequences identified through combinatorial means to bind to one of three closely related photosensitizers *m*-THPC, Chlorin E6 (Ce6), and Pheophorbide A (Pb*a*) (cf. Figure 1). The objective was to evaluate the capability of the

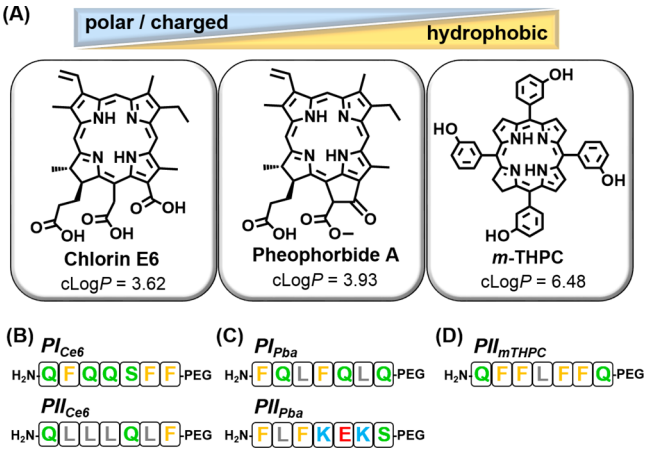

Figure 1. (A) Structures of screened photosensitizers Chlorin E6, Pheophorbide A, and *m*-THPC. Amino acid sequences of potential peptide-PEG conjugate solubilizers for (B) Chlorin E6 ($\mathbf{PI}_{Ce6}$ and $\mathbf{PII}_{Ce6}$), (C) Pheophorbide A ($\mathbf{PI}_{Pba}$ and $\mathbf{PII}_{Pba}$), and (D) the reference conjugate found for *m*-THPC ($\mathbf{PII}_{mTHPC}$).

screening procedure to read out minor structural changes between small-molecule drugs and deliver peptides that reflect those differences within the amino acid sequences. Furthermore, insights into peptide-drug host−guest interactions at the molecular level will be provided by means of systematic amino acid point mutations (Alanine scans) and computational binding studies.

RESULTS AND DISCUSSION

The competitive study investigated three photosensitizers, which all possess the chlorin scaffold and only differ in the type and orientation of the peripheral substituents (Figure 1A). *m*-THPC has four symmetric hydroxyphenyl substituents in the *meso*-position of the chlorin structure. Ce6 and Pb*a* are both unsymmetrically substituted and present on one side of the planar aromatic scaffold hydrophobic methyl, ethyl, and vinyl groups, whereas on the opposite side polar/charged functionalities are pendent. Pb*a* displays one carboxyl, an ester, and a ketone functionality, whereas Ce6 shows three carboxyl groups, making Ce6 the most water-soluble compound of the three sensitizers. The increase in polarity of the photosensitizers is reflected in a decrease of the partitioning coefficients that were calculated for cLogP $_{m\text{-THPC}}$ = 6.48, cLogP $_{Pba}$ = 3.93, and cLogP $_{Ce6}$ = 3.62.

The screening of appropriate peptide binders for *m*-THPC has been reported recently.[31] For direct comparison, the same screening assay and identical peptide library were applied to select peptidic binding partners for Ce6 and Pb*a*. By following the procedure originally developed for *m*-THPC, a one-bead-one-compound peptide library with about 8.2 × 10^5 7mer sequences constituted from seven different amino acids (F, L, G, K, Q, S, E) was incubated with either Ce6 or Pb*a*. The partitioning of the drugs in the library and the enrichment of the sensitizers at certain beads, which present suitable peptides, was followed by fluorescence microscopy at excitation of 668 and 674 nm for Ce6 and Pb*a*, respectively (SI, Figure S1). For both sensitizers, 40 positive beads were selected, the peptides were isolated after cleavage from the supports by cyanogen bromide,[31,47] and MALDI-ToF-MS/MS revealed amino acid sequences suitable for drug binding. A clear enrichment of aromatic Phe, hydrophobic Leu, and polar Gln residues is evident (SI Tables S1 and S2). In direct comparison to sequences found for *m*-THPC binders, the Phe residue is slightly less enriched, but the more polar Ser was found to be more present for both Ce6 and Pb*a* (SI Figure S2). This may reflect the absence of the aromatic substituents from *m*-THPC, making hydrogen bonding more relevant for interactions with Ce6 and Pb*a*.

From those screening results, two amino acid sequences were selected for each sensitizer compound, and the corresponding peptide-poly(ethylene glycol) peptide-PEG conjugates were synthesized (Figure 1). H_2N-QFQQSFF-PEG ($\mathbf{PI}_{Ce6}$) and H_2N-QLLLQLF-PEG ($\mathbf{PII}_{Ce6}$) represent peptide binders for Ce6 that reflect the obvious importance of Gln and Leu residues for interactions with Ce6 as evidenced by the screening results. Furthermore, $\mathbf{PI}_{Ce6}$ includes three aromatic Phe residues, which might facilitate $\pi-\pi$-stacking between peptide and chlorin scaffold of the photosensitizer. Interestingly, $\mathbf{PII}_{Ce6}$ contains four Leu, one Phe, and two Gln residues, which have been proven to be relevant for hosting *m*-THPC (cf. $\mathbf{PII}_{mTHPC}$, H_2N-QFFLFFQ-PEG).[31] Counterintuitively, the set of Ce6 binders was not dominantly enriched with Lys as cationic residue enabling Coulombic interactions. This might point to strong intramolecular interactions of the three carboxyl functionalities in Ce6. For Pb*a* binders the peptide-PEG conjugates H_2N-FQLFQLQ-PEG ($\mathbf{PI}_{Pba}$) and H_2N-FLFKEKS-PEG ($\mathbf{PII}_{Pba}$) were selected, exhibiting also Phe, Leu, and Gln residues. While for Pb*a* binders similar residues are selected compared to $\mathbf{PII}_{mTHPC}$, no central hydrophobic and aromatic block segments are found. Instead, Phe and Leu residues were

DOI: 10.1021/acs.bioconjchem.6b00549
Bioconjugate Chem. 2017, 28, 760−767

consistently separated by polar Gln residues. **PII$_{Pba}$** comprises a polar and charged *C*-terminus with two Lys and a Glu residue, whereas *N*-terminal a hydrophobic FLF trimer is found. This sequence was studied since within the screening several peptides with charged Lys residues in the *C*-terminal region were selected (cf. SI). These sequence constitutions potentially allow for hydrogen bonding to the Pb*a* carboxyl function, whereas the *N*-terminal hydrophobic trimer makes $\pi-\pi$-stacking with the aromatic scaffold of Pb*a* feasible.

The peptide conjugates were loaded with the sensitizers following a modified forced loading protocol, developed for *m*-THPC (cf. SI).[31] Briefly, Ce6 or Pb*a* were dissolved in DMSO and solutions of the corresponding peptide-PEG conjugates in water were added, followed by freeze-drying in vacuo. The dry mixture was resuspended in water, and not solubilized sensitizer was removed by centrifugation. Concentration determination of solubilized drug molecules was performed by means of UV−vis absorption spectroscopy.

In general, the screening procedure provides peptide sequences that allow for the effective solubilization of the particular target drug, which has been used in the selection process (cf. Figure 2). **PI$_{Ce6}$** was able to solubilize 0.56 mmol Ce6 per mmol carrier (1:1.8 molar drug/carrier ratio), whereas **PII$_{Ce6}$** showed only a concentration of 0.02 mmol Ce6 per mmol carrier (1:50 molar drug/carrier ratio). Apparently, a high number of aromatic and polar side chain functionalities such as Phe and Gln residues seem to be favorable for solubilization of Ce6 compared to a high content of hydrophobic Leu residues (cf. **PI$_{Ce6}$** versus **PII$_{Ce6}$**). In the case of Pb*a*, **PI$_{Pba}$** and **PII$_{Pba}$** were able to solubilize 0.45 and 0.42 mmol per mmol carrier, respectively (1:2.2 and 1:2.4 molar ratio). Again, the combination of Phe, Leu, and Gln (**PI$_{Pba}$**) proved to be successful for solubilization of the sensitizer. Interestingly, **PII$_{Pba}$**, which carries only a rather small aromatic and hydrophobic FLF-trimer at the *N*-terminus but the charged and polar tetramer KEKS at the *C*-terminus, was almost as effective in hosting Pb*a* as the carrier **PI$_{Pba}$**. This is noteworthy, since Lys residues particularly proved to be unfavorable for both Ce6 and *m*-THPC solubilization. Altogether, the de novo solubilizers **PI$_{Ce6}$** and **PI$_{Pba}$** have been identified, showing rather good drug loading abilities for their individual drugs Ce6 and Pb*a*, respectively, if compared to **PII$_{mTHPC}$** found for *m*-THPC. For both **PI$_{Ce6}$** and **PI$_{Pba}$** payload capacities are reached that even slightly exceed those found for the *m*-THPC solubilizer **PII$_{mTHPC}$** (0.31 mmol/mmol conjugate, 1:3.3 molar ratio). Commonly established amphiphilic block copolymer-based formulation additives such as Pluronics F68 or P123 might show under some conditions even higher payload capacities for certain hydrophobic photosensitizers.[48] However, the strong drug binding is based on nonspecific, entropic interactions and could lead to slow trans-solubilization kinetics[31] that might cause extended light sensitivity in patients after treatment.

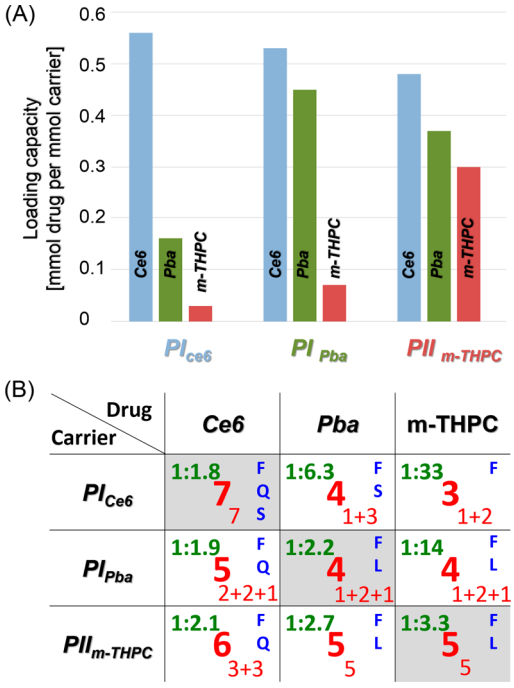

Figure 2. Reachable maximum loading capacities of three different drugs Ce6, Pb*a*, and *m*-THPC solubilized by the three different solubilizer conjugates **PI$_{Ce6}$**, **PI$_{Pba}$**, and **PII$_{mTHPC}$** (A) and solubilization matrix (B) summarizing obtained drug:carrier ratio (green), type, and number of anticipated amino acid residues that meet characteristics of the different drug structures (blue-type and red-number with subscript showing occurrence of relevant residues in noninterrupted manner).

Despite the fact that a linear screening assay was performed for each of the drugs and drug selectivity has not been introduced during the screening in form of any selection pressure, the drug selectivity of the newly identified peptides were evaluated. For that purpose, the three most promising solubilizers **PI$_{Ce6}$**, **PI$_{Pba}$**, and **PII$_{mTHPC}$** were studied to solubilize the respective set of off-target photosensitizers Ce6, Pb*a*, and *m*-THPC. The resulting solubilization matrix is summarized in Figure 2 (cf. SI Table S4).

Considering the small size of the 7mer binding domains, a remarkable and clear tendency is evident. It is noteworthy that the screening procedure delivers de novo solubilizers, which show the best performance for the target drugs. Conclusively, the highest payload of Ce6 is found for **PI$_{Ce6}$**, Pb*a* is solubilized best with **PI$_{Pba}$** and most *m*-THPC is solubilized by **PII$_{mTHPC}$**. This highlights the potential of the screening procedure to select peptide sequences specifically adapted for the targets to solubilize particular drug molecules. Beyond this, the hydrophobicity/hydrophilicity match of the solubilizer peptides and the different drug cargos also seems to be of importance. **PI$_{Ce6}$** and **PI$_{Pba}$** were selected for more polar drug candidates. Hence compared to **PII$_{mTHPC}$** both **PI$_{Ce6}$** and **PI$_{Pba}$** show most obvious selectivity for their respective target drugs as the hydrophobic *m*-THPC was practically not solubilized (target: **PII$_{mTHPC}$**/*m*-THPC 1:3.3 versus off-target: **PI$_{Ce6}$**/*m*-THPC 1:33 and **PI$_{Pba}$**/*m*-THPC 1:14 (molar ratio drug:carrier)). The differentiation between the structurally more closely related Ce6 and Pb*a* entities, however, appears to be most challenging. Where **PI$_{Ce6}$** strongly favors Ce6 over Pb*a* (1:1.8 and 1:6.3), the **PI$_{Pba}$** conjugate shows a slightly higher capacity to bind the off-target Ce6 compared to the target Pb*a* (1:1.9 and 1:2.2). **PII$_{mTHPC}$** was found for the most hydrophobic photosensitizer, and therefore it seems to be understandable that both Ce6 and Pb*a* can interact with the binding peptide most likely via nonsequence specific hydrophobic/entropic interactions. This is reflected in the payload values obtained for **PII$_{mTHPC}$** off-target capacities 1:2.1 (Ce6) and 1:2.7 (Pb*a*) compared to the target capacity of 1:3.3 for *m*-THPC.

It should be emphasized that despite the structural relation of Ce6, Pb*a*, and *m*-THPC as well as the similarities in amino acid

DOI: 10.1021/acs.bioconjchem.6b00549
Bioconjugate Chem. 2017, 28, 760−767

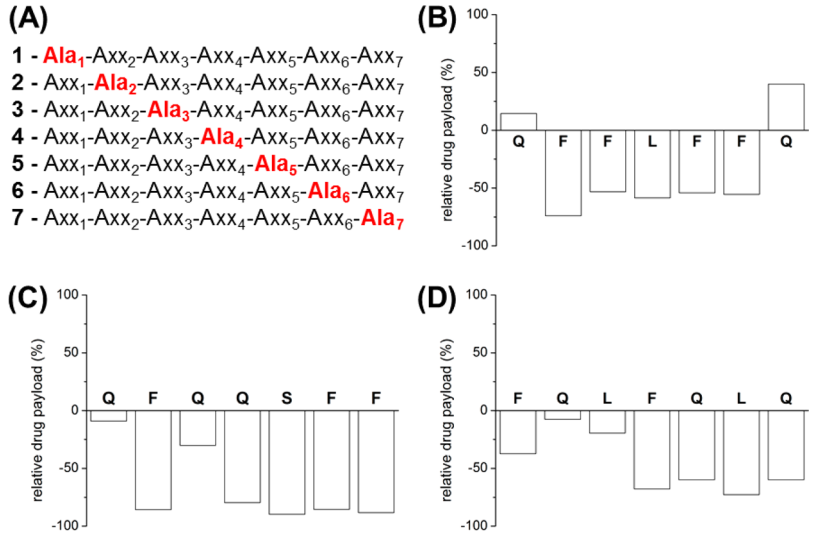

Figure 3. Effect of amino acid sequence positions on maximum drug payload by comparing the maximal loading of a set of point-mutated conjugate solubilizers (A) to their parent compounds. Changes in relative payload obtained by $\mathbf{PII}_{\mathbf{mTHPC}}$/*m*-THPC (B), $\mathbf{PI}_{\mathbf{Ce6}}$/Ce6 (C), and $\mathbf{PI}_{\mathbf{Pb}a}$/Pb*a* (D).

residues that compose the short 7mer sequences of $\mathbf{PII}_{\mathbf{mTHPC}}$, $\mathbf{PI}_{\mathbf{Ce6}}$, and $\mathbf{PI}_{\mathbf{Pb}a}$ some effects on drug-tailored binding are evident. Clearly, the applied screening procedure and the peptide length are limiting the specificity reachable to distinguish between the drug entities. Hence, the contacts between de novo solubilizers and drugs are certainly far away from molecular recognition events. Those, however, are also not needed in these particular transport solubilizer systems.

The differences in payload and apparent drug selectivity within the set of conjugate solubilizers might be rationalized by taking amino acid residues into account, which meet characteristics of the different drug structures (cf. Figure 2B). Based on the occurrence of Phe residues, $\pi-\pi$-stacking interactions with the chlorin scaffolds are relevant for each of these drugs. Moreover, following the increase in hydrophobicity from Ce6 to Pb*a* to *m*-THPC, a general decrease in the importance of polar amino acid residues such as Gln and Ser could be anticipated, which is in line with an increase in the importance of the hydrophobic Leu residue. As summarized in Figure 2, maximum capacity for the most polar Ce6 and most nonpolar *m*-THPC can be expected, when a maximum number of relevant residues are occurring in a blocked, noninterrupted manner. The small 3 × 3 matrix of peptide sequences and drugs does not offer the full picture, but a reduction of both the number of relevant amino acid residues and the continuous occurrence of these residues in the sequences indicate a negative effect on the solubilization behavior.

To evaluate the contribution of amino acid residues at specific sequence positions to the overall drug loading capacity, systematic residue point mutations (alanine scan) of $\mathbf{PII}_{\mathbf{mTHPC}}$, $\mathbf{PI}_{\mathbf{Ce6}}$, and $\mathbf{PI}_{\mathbf{Pb}a}$ were synthesized and investigated (cf. Figure 3). This study gave rise to a set of seven mutated conjugate carriers per photosensitizer (cf. SI). The Ala-containing conjugates were loaded with their respective target drug and loading capacities were compared to that of the wild-type reference conjugate (Figure 3).

The investigation of the point-mutated solubilizers originating from the conjugate $\mathbf{PII}_{\mathbf{mTHPC}}$ revealed the obvious importance of hydrophobic and $\pi-\pi$-stacking interactions as the main driving force for solubilizing *m*-THPC. Replacing one of the aromatic Phe residues or the central Leu by Ala is followed by a substantial loss in payload capacity, whereas *N*- or *C*-terminal polar Gln residue substitution showed enhanced solubilization efficiency. This behavior was expected since *m*-THPC exhibits a highly hydrophobic and aromatic structure compared to Ce6 and Pb*a* with four equal hydroxyphenyl substituents in *meso*-position. Surprisingly, for $\mathbf{PI}_{\mathbf{Ce6}}$ and $\mathbf{PI}_{\mathbf{Pb}a}$ replacing polar Gln and Ser residues by Ala, especially close to the PEG-connected *C*-terminus, showed a dramatic reduction of the payload capacity compared to a Phe and Leu substitution. Close to the *N*-terminus, however, the effect is almost negligible. It is noteworthy that Gln_4 and Ser_5 for $\mathbf{PI}_{\mathbf{Ce6}}$, as well as Gln_5 and Gln_7 for $\mathbf{PI}_{\mathbf{Pb}a}$, apparently contribute as much to drug binding as the aromatic Phe residues in the sequences. This is pointing out the importance of H-bonds for the binding and solubilization of the more polar photosensitizers Ce6 and Pb*a*, whereas residues with H-bond donor and acceptor side-chain functionalities can be neglected for *m*-THPC binding.

As previously shown, *m*-THPC was solubilized by peptide-PEG conjugates in the core of colloidal aggregates, exhibiting a silent, inactivated drug state.[31] To elucidate potential differences in modes of solubilization, which could be the origin for differences in drug payload, cryogenic transmission electron microscopy (cryo-TEM) was utilized to investigate aggregate formation of the selected conjugate solubilizers and their respective target drugs (cf. SI Table S5). Irrespective of the peptide segment, all solubilizers $\mathbf{PI}_{\mathbf{Ce6}}$ and $\mathbf{PI}_{\mathbf{Pb}a}$ and $\mathbf{PII}_{\mathbf{mTHPC}}$ behave in a similar manner in the absence of their cargo. Colloidal aggregates with radii in the range of about R_{TEM} = 5−17 nm could be observed. These globular aggregates in each sample are well-dispersed and nonagglomerated, and the sizes found are too large to correspond to a classical micellar aggregate form. After drug loading, the aggregates remain fairly globular, and the size of the primary colloids increases only slightly to R_{TEM} = 7−19 nm in the case of both $\mathbf{PI}_{\mathbf{Ce6}}$/Ce6 and $\mathbf{PI}_{\mathbf{Pb}a}$/Pb*a* complexes and larger objects with R_{TEM} of up to 24 nm could be found for $\mathbf{PII}_{\mathbf{mTHPC}}$/*m*-THPC complexes. The cryo-TEM micrographs indicate for all drug complexes investigated a tendency to agglomerate to larger colloidal clusters. In fact, such a mode of stabilization of additional hydrophobic interfaces could be expected, as the sizes of the

DOI: 10.1021/acs.bioconjchem.6b00549
Bioconjugate Chem. 2017, 28, 760−767

primary colloids are not dramatically changing even at high cargo load of 1:2 as found in $\mathbf{PI}_{Pba}$/Pb*a* complexes. Dynamic light scattering measurements of solutions of all drug-loaded samples indicated average complex sizes below R_h < 100 nm and hence confirm a window suitable for biomedical applications (cf. SI Table S5).

To gain insight into the putative noncovalent interactions between the cargo and the carrier peptides at a molecular level, molecular-modeling studies were performed by using the MAB force field implemented in the software MOLOC.[49] Idealized 1:1 complexes of Pb*a* and Ce6 with the corresponding peptides were modeled. The C-terminal PEG moieties of the solubilizers were reduced to a single oligo(ethylene glycol) unit for ease of computational accessibility as PEG-drug interactions can be neglected. Figure 4 shows the two preferential dispositions of

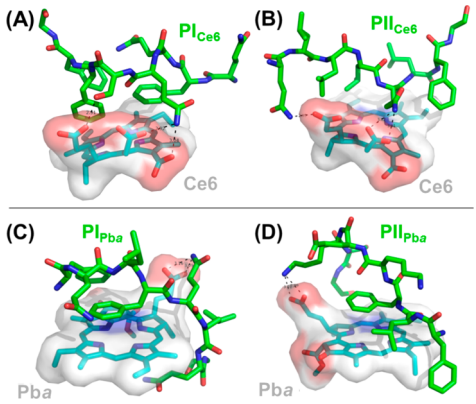

Figure 4. Idealized binding studies of the drugs Chlorin E6 or Pheophorbide A (blue sticks and van der Waals surface) with peptide segments from of the respective bioconjugates ($\mathbf{PI}_{Ce6}$, $\mathbf{PII}_{Ce6}$, $\mathbf{PI}_{Pba}$, $\mathbf{PII}_{Pba}$ - green sticks) as 1:1 complexes ((A) $\mathbf{PI}_{Ce6}$/Ce6, (B) $\mathbf{PII}_{Ce6}$/Ce6, (C) $\mathbf{PI}_{Pba}$/Pb*a*, and (D) $\mathbf{PII}_{Pba}$/Pb*a*; the images were obtained using *PYMOL*).

the peptides around Pba and Ce6 that were found in each case. Generally speaking, when hydrophobic residues are not involved in direct interactions with the cargo, they are engaged in intramolecular hydrophobic contacts, contributing indirectly to the stabilization of the drug/carrier complex.

The modeled interaction of Ce6 with $\mathbf{PI}_{Ce6}$ is apparently dominated, besides $\pi-\pi$–stacking with Phe residues, by the formation of a complex network of H-bonding interactions that are mediated by the side chains of Gln_4 and Ser_5 residues that are in proximity of Ce6. A similar pattern of H-bonding interactions is observed also in the predicted interaction modes for the complex $\mathbf{PII}_{Ce6}$/Ce6. Moreover, two out of the four Leu residues of $\mathbf{PII}_{Ce6}$ interact directly with Ce6, while one is engaged in intramolecular hydrophobic contacts leaving the fourth Leu residue solvent-exposed. The computational models suggest that for Pb*a*, a sandwich-type complex is possible with $\mathbf{PI}_{Pba}$, in which Pb*a* is involved in $\pi-\pi$-stacking interactions with the side chain of a Phe residue and with the side-chain amide moiety of a Gln residue. Two H-bonding interactions with the carboxylate moiety of Pb*a* anchor the peptide to Pb*a*, favoring the positioning of the peptide around Pb*a* for the formation of a sandwich-type complex. For the complex $\mathbf{PII}_{Pba}$/Pb*a*, a stable sandwich-type complex could not be found. However, the predicted complex is stabilized by numerous hydrophobic contacts. Also, in this case, the peptide is anchored to Pb*a* through a hydrogen-bonding interaction between the carboxylate moiety of Pb*a* and the side-chain amino group of a Lys residue. While for $\mathbf{PII}_{Pba}$/Pb*a* and $\mathbf{PI}_{Ce6}$/Ce6, stoichiometric 1:1 complexes might be feasible according to our modeling studies, in the case of $\mathbf{PI}_{Pba}$/Pb*a* and $\mathbf{PII}_{Ce6}$/Ce6 the presence of hydrophobic yet solvent-exposed residues might suggest that a stoichiometric 1:1 complex formation between the drug and host peptide is unlikely to occur. Interestingly, results of modeling studies are in very good agreement with $\mathbf{PI}_{Ce6}$ and $\mathbf{PI}_{Pba}$ alanine scans (Figure 3 and SI Figure S32). Substitution of Gln_1 and Gln_3 in $\mathbf{PI}_{Ce6}$ had only a minor effect on the payload capacity. Modeling showed a binding mode where these residues are both pointing away from the drug molecule and do not contribute to Ce6 binding. This is equally the case for Gln_2 and Leu_3 of $\mathbf{PI}_{Pba}$. Whereas *N*-terminal Gln and Leu residues proved to be important, Gln_2 and Leu_3 show no noticeable interaction with Pb*a*. Together with the cross solubilization experiment between $\mathbf{PI}_{Ce6}$, $\mathbf{PI}_{Pba}$, and $\mathbf{PI}_{mTHPC}$, Ala-scanning and modeling studies highlight the sequence-dependent specific interaction between screened drug moiety and tailor-made conjugate carrier. It should be noted that the revealed binding interactions in the different 1:1 solubilizer/drug complexes only have model character. The findings are, however, consistent with observations from the alanine scans. Therefore, the interaction modes observed within the computational study are probably more likely to occur in the actual colloidal drug-solubilizer aggregates.

In conclusion, the screening of an immobilized one-bead-one-compound peptide library against a set of small-molecule drugs proved to be capable of reading out structural differences of the three related chlorin-based photosensitizers, having different substitution patterns. The peptide sequences identified were integrated into peptide-poly(ethylene glycol) (peptide-PEG) conjugates to act as effective solubilizers for the respective drug the screening has been performed with. While the target chlorin drug was always best solubilized by the identified peptide-PEG conjugates, additional selectivity for solubilization of related off-target drugs could be found, depending on the peptide sequences and polarity contrasts. Despite the fact that the screening was not performed to identify drug binders, which discriminate between drug structures as no selection pressure was used to evolve the system in this direction, some remarkable selectivity effects could be observed. Failures of the Ce6-solubilizer $\mathbf{PI}_{Ce6}$ and the Pba-solubilizer $\mathbf{PI}_{Pba}$ to solubilize reasonable amounts of *m*-THPC were obvious. Moreover, for $\mathbf{PI}_{Ce6}$ significant binding capacity differences reveals differentiation between the structurally closely related Ce6 and Pb*a* drugs to underline the precision of binding between drug and carrier already at a level of short 7mer peptides. An alanine scan of the binding peptides was in excellent agreement with the computational modeling study, where residues that proved to be of lower importance regarding drug payload capacity also show no obvious interaction with the computational simulations. Interestingly, specific interactions in guest/host systems can be realized already by 7mer interaction domains and do not necessarily require the design of complex proteins. This offers opportunities to equip existing polymer-based drug-delivery systems with advanced functions for drug-specific transport.

■ EXPERIMENTAL PROCEDURES

Detailed description of materials, instrumentation, experimental procedures, and analytical data are available as Supporting Information.

DOI: 10.1021/acs.bioconjchem.6b00549
Bioconjugate Chem. 2017, 28, 760−767

The peptide library for screening against Chlorin E6 and Pheophorbide A was prepared as previously described[31] on Aminomethyl-ChemMatrix resin through manual single coupling (Fmoc strategy) using PyBOP and DIPEA in NMP. The resin was acetylated with Ac_2O and DIPEA in NMP after each coupling step and Fmoc deprotection was achieved by treatment with piperidine (20%) in NMP. First, a cleavable linker sequence (Gly-Gly-Met) was synthesized on the resin, followed by a randomized 7mer sequence by split&mix technique containing Gly, Leu, Phe, Glu, Lys, Ser, Gln at each position.[33] Finally, the resin was treated with a mixture of 94% TFA, 2.5% TES, 2.5% EDT, and 1% deionized water to remove side chain protecting groups.

The resin-bound peptide library was incubated with Chlorin E6 or Pheophorbide A (1.5 mmol/L) in a mixture of deionized water and EtOH (9:1 v/v) for 72 h. Drug enrichment on beads carrying a peptide sequence with high affinity to noncovalent drug binding was followed via fluorescence microscopy (cf. SI Figure S1) using a *Zeiss Axio* fluorescence microscope (Carl Zeiss MicroImaging GmbH). Fluorescing beads were removed from suspension, and peptides were cleaved from the solid support via treatment with CNBr in 0.1 M HCl at RT overnight. To distinguish Gln and Lys in MS analysis, peptides were acetylated with Ac_2O/AcOH in acetone. Sequencing was performed with a 5800 MALDI ToF/ToF system (AB SIEX) using AHCA as matrix. Sequences were determined using a MASCOT Server (Matrix Science Ltd.) for database search from a custom-made file containing all theoretically possible peptide sequences (823 543 different sequences). Sequencing results are summarized in Table S1 and Table S2 (cf. SI).

Peptide-PEG conjugates (PI_{Ce6}, PII_{Ce6}, PI_{Pba}, PII_{Pba}, and PII_{mTHPC}) were obtained by automated solid-phase peptide synthesis on an ABI 433a peptide synthesizer (Applied Biosystems) using Tentagel-PAP resins as solid support preloaded with PEG (approximately 3.2 kg/mol) via HBTU/NMP/piperidine protocol. Alanine scan conjugate synthesis was performed by using a MultiPep RS parallel synthesizer (Intavis Bioanalytical Instruments AG), where coupling was performed by preactiviation of amino acid derivatives with HCTU, Oxyma Pure, and NMM in DMF and Fmoc deprotection with 20% piperidine in DMF. Conjugates were cleaved from the solid support by treatment with a mixture of 97% TFA, 2% TES, and 1% H_2O, precipitated in cold diethyl ether and dialyzed against deionized water (100−500 or 500−1000 Da MWCO, cellulose ester). Peptide conjugates were characterized by MALDI-ToF-MS, ^{1}H nuclear magnetic resonance spectra (^{1}H NMR) in TFA-d1, and Fourier transform infrared spectroscopy (ATR-FT-IR, cf. SI).

For solubilization of sensitizers by peptide-PEO conjugates *m*-THPC was dissolved in EtOH (1 mg/mL), Chlorin E6, and Pheophorbide A in DMSO. One milliliter aliquots of the drug solutions (1.47 μmol drug) were added to solutions of each carrier containing 1.47 μmol conjugate in deionized water (1 mL, pH 7). The resulting mixtures were shaken for 1 h and freeze-dried in vacuo. Residues were dissolved in deionized water (1 mL, pH 7), followed by centrifugation to remove drug which was not solubilized. Supernatants were diluted with EtOH or DMSO (1:100 v/v), respectively, to avoid aggregation, and concentration of solubilized drug was determined by UV−vis spectroscopy.

The three-dimensional structures of the peptides $PI{-}II_{Ce6}$ and $PI{-}II_{Pba}$ were generated using the software CORINA,[50] and docked onto the structure of Ce6 and Pb*a*. Idealized 1:1 complexes of Ce6 or Pb*a* and peptides $PI{-}II_{Ce6}$ and $PI{-}II_{Pba}$ have been taken into account. The energy of the peptide−Ce6 (or Pb*a*) complexes was minimized using the MAB force field as implemented in the computer program MOLOC,[49] while keeping the coordinates of Ce6 and Pb*a* fixed. During the modeling, the PEG chain was taken into account as a single unit.

■ ASSOCIATED CONTENT

Supporting Information

The Supporting Information is available free of charge on the ACS Publications website at DOI: 10.1021/acs.bioconjchem.6b00549.

Materials, instrumentation, experimental procedures, and analytical data (PDF)

■ AUTHOR INFORMATION

Corresponding Author

*E-mail: h.boerner@hu-berlin.de. Phone: +49 (0)30-2093 7348. Fax: +49 (0)30 2093-7500.

ORCID

Anna K. H. Hirsch: 0000-0001-8734-4663

Hans G. Börner: 0000-0001-9333-9780

Notes

The authors declare no competing financial interest.

■ ACKNOWLEDGMENTS

H.G.B. would like to acknowledge funding granted by the European Research Council under the European Union's seventh Framework Program (FP07−13)/ERC Starting grant "Specifically Interacting Polymers − SIP" (ERC 305064), by the School of Analytical Sciences Adlershof (SALSA) in the framework of the German Excellence Initiative and the German Research Council DFG under the SFB1112 "Nanocarriers". A.K.H.H. acknowledges the Dutch Ministry of Education, Culture, Science (gravitation program 024.001.035). We acknowledge M. Senge (Trinity College Dublin) for providing *m*-THPC, K. Linkert (HU) for SPPS, M. Ballauff for EM access, S. M. Weidner (BAM) for MALDI access, and H. Stephanowitz as well as E. Krause for MALDI-MS/MS-sequencing.

■ REFERENCES

(1) Paul, S. M., Mytelka, D. S., Dunwiddie, C. T., Persinger, C. C., Munos, B. H., Lindborg, S. R., and Schacht, A. L. (2010) How to improve R&D productivity: the pharmaceutical industry's grand challenge. *Nat. Rev. Drug Discovery 9*, 203−214.

(2) DiMasi, J. A., Hansen, R. W., and Grabowski, H. G. (2003) The price of innovation: new estimates of drug development costs. *J. Health Econ. 22*, 151−185.

(3) Williams, H. D., Trevaskis, N. L., Charman, S. A., Shanker, R. M., Charman, W. N., Pouton, C. W., and Porter, C. J. H. (2013) Strategies to Address Low Drug Solubility in Discovery and Development. *Pharmacol. Rev. 65*, 315−499.

(4) Petros, R. A., and DeSimone, J. M. (2010) Strategies in the design of nanoparticles for therapeutic applications. *Nat. Rev. Drug Discovery 9*, 615−627.

(5) Duncan, R. (2003) The dawning era of polymer therapeutics. *Nat. Rev. Drug Discovery 2*, 347−360.

(6) Schoonen, L., and van Hest, J. C. M. (2014) Functionalization of protein-based nanocages for drug delivery applications. *Nanoscale 6*, 7124−7141.

DOI: 10.1021/acs.bioconjchem.6b00549
Bioconjugate Chem. 2017, 28, 760−767

(7) Kataoka, K., Harada, A., and Nagasaki, Y. (2001) Block copolymer micelles for drug delivery: design, characterization and biological significance. *Adv. Drug Delivery Rev. 47*, 113−131.
(8) Hirsch, A. K. H., Diederich, F., Antonietti, M., and Börner, H. G. (2010) Bioconjugates to specifically render inhibitors water-soluble. *Soft Matter 6*, 88−91.
(9) Torchilin, V. P. (2006) Micellar nanocarriers: Pharmaceutical perspectives. *Pharm. Res. 24*, 1−16.
(10) Esfand, R., and Tomalia, D. A. (2001) Poly(amidoamine) (PAMAM) dendrimers: from biomimicry to drug delivery and biomedical applications. *Drug Discovery Today 6*, 427−436.
(11) Alconcel, S. N. S., Baas, A. S., and Maynard, H. D. (2011) FDA-approved poly(ethylene glycol)-protein conjugate drugs. *Polym. Chem. 2*, 1442−1448.
(12) Zhang, F., Zhang, S., Pollack, S. F., Li, R., Gonzalez, A. M., Fan, J., Zou, J., Leininger, S. E., Pavía-Sanders, A., Johnson, R., et al. (2015) Improving Paclitaxel Delivery: In Vitro and In Vivo Characterization of PEGylated Polyphosphoester-Based Nanocarriers. *J. Am. Chem. Soc. 137*, 2056−2066.
(13) Synatschke, C. V., Nomoto, T., Cabral, H., Förtsch, M., Toh, K., Matsumoto, Y., Miyazaki, K., Hanisch, A., Schacher, F. H., Kishimura, A., et al. (2014) Multicompartment Micelles with Adjustable Poly(ethylene glycol) Shell for Efficient in Vivo Photodynamic Therapy. *ACS Nano 8*, 1161−1172.
(14) Fleige, E., Quadir, M. A., and Haag, R. (2012) Stimuli-responsive polymeric nanocarriers for the controlled transport of active compounds: Concepts and applications. *Adv. Drug Delivery Rev. 64*, 866−884.
(15) Peer, D., Karp, J. M., Hong, S., Farokhzad, O. C., Margalit, R., and Langer, R. (2007) Nanocarriers as an emerging platform for cancer therapy. *Nat. Nanotechnol. 2*, 751−760.
(16) He, Z., Schulz, A., Wan, X., Seitz, J., Bludau, H., Alakhova, D. Y., Darr, D. B., Perou, C. M., Jordan, R., Ojima, I., et al. (2015) Poly(2-oxazoline) based micelles with high capacity for 3rd generation taxoids: Preparation, in vitro and in vivo evaluation. *J. Controlled Release 208*, 67−75.
(17) Brinkhuis, R. P., Rutjes, F. P. J. T., and van Hest, J. C. M. (2011) Polymeric vesicles in biomedical applications. *Polym. Chem. 2*, 1449−1462.
(18) Birke, A., Huesmann, D., Kelsch, A., Weilbächer, M., Xie, J., Bros, M., Bopp, T., Becker, C., Landfester, K., and Barz, M. (2014) Polypeptoid-block-polypeptide Copolymers: Synthesis, Characterization, and Application of Amphiphilic Block Copolypept(o)ides in Drug Formulations and Miniemulsion Techniques. *Biomacromolecules 15*, 548−557.
(19) Jonker, A. M., Lowik, D., and van Hest, J. C. M. (2012) Peptide- and Protein-Based Hydrogels. *Chem. Mater. 24*, 759−773.
(20) Schnitzler, T., and Herrmann, A. (2012) DNA Block Copolymers: Functional Materials for Nanoscience and Biomedicine. *Acc. Chem. Res. 45*, 1419−1430.
(21) Hamley, I. W. (2015) Lipopeptides: from self-assembly to bioactivity. *Chem. Commun. 51*, 8574−8583.
(22) Börner, H. G., Kühnle, H., and Hentschel, J. (2010) Making "Smart Polymers" Smarter: Modern Concepts to Regulate Functions in Polymer Science. *J. Polym. Sci., Part A: Polym. Chem. 48*, 1−14.
(23) Desseaux, S., Hinestrosa, J. P., Schuwer, N., Lokitz, B. S., Ankner, J. F., Kilbey, S. M., Voitchovsky, K., and Klok, H. A. (2016) Swelling Behavior and Nanomechanical Properties of (Peptide-Modified) Poly(2-hydroxyethyl methacrylate) and Poly(poly(ethylene glycol) methacrylate) Brushes. *Macromolecules 49*, 4609−4618.
(24) Gentsch, R., Boysen, B., Lankenau, A., and Börner, H. G. (2010) Single-step electrospinning of bimodal fiber meshes for ease of cellular infiltration. *Macromol. Rapid Commun. 31*, 59−64.
(25) Schwemmer, T., Baumgartner, J., Faivre, D., and Börner, H. G. (2012) Peptide-mediated nanoengineering of inorganic particle surfaces: A general route toward surface functionalization via peptide adhesion domains. *J. Am. Chem. Soc. 134*, 2385−2391.
(26) Samsoninkova, V., Seidt, B., Hanßke, F., Wagermaier, W., and Börner, H. G. (2016) Peptide-polymer conjugates for bio-inspired compatibilization of internal composite interfaces: Via specific interactions toward stiffer and tougher materials. *Adv. Mater. Interfaces*, 1600501.
(27) Wilke, P., Helfricht, N., Mark, A., Papastavrou, G., Faivre, D., and Börner, G. H. (2014) A direct biocombinatorial strategy towards next generation, mussel-glue inspired saltwater adhesives. *J. Am. Chem. Soc. 136*, 12667−12674.
(28) Dünne, A. A., Börner, H. G., Kukula, H., Schlaad, H., Werner, J. A., Wiegand, S., and Antonietti, M. (2007) Block copolymer carrier systems for translymphatic chemotherapy of lymph node metastases. *Anticancer Res. 27*, 3935−3940.
(29) Bode, S. A., Hansen, M. B., Oerlemans, R., van Hest, J. C. M., and Lowik, D. (2015) Enzyme-Activatable Cell-Penetrating Peptides through a Minimal Side Chain Modification. *Bioconjugate Chem. 26*, 850−856.
(30) Hartmann, L., Häfele, S., Peschka-Suess, R., Antonietti, M., and Börner, H. G. (2008) Tailor-made poly(amidoamine)s for controlled complexation and condensation of DNA. *Chem. - Eur. J. 14*, 2025−2033.
(31) Wieczorek, S., Krause, E., Hackbarth, S., Röder, B., Hirsch, A. K. H., and Börner, H. G. (2013) Exploiting Specific Interactions toward Next-Generation Polymeric Drug Transporters. *J. Am. Chem. Soc. 135*, 1711−1714.
(32) Lawatscheck, C., Pickhardt, M., Wieczorek, S., Grafmüller, A., Mandelkow, E., and Börner, H. G. (2016) Generalizing the concept of specific compound formulation additives toward non-fluorescent drugs: A solubilization study on potential anti-Alzheimer active small molecule compounds. *Angew. Chem., Int. Ed. 55*, 8752−8756.
(33) Lam, K. S., Salmon, S. E., Hersh, E. M., Hruby, V. J., Kazmierski, W. M., and Knapp, R. J. (1991) A new type of synthetic peptide library for identifying ligand-binding activity. *Nature 354*, 82−84.
(34) Senge, M. O., and Brandt, J. C. (2011) Temoporfin (Foscan (R), 5,10,15,20-Tetra(m-hydroxyphenyl)chlorin)-A Second-generation Photosensitizer. *Photochem. Photobiol. 87*, 1240−1296.
(35) Paszko, E., Ehrhardt, C., Senge, M. O., Kelleher, D. P., and Reynolds, J. V. (2011) Nanodrug applications in photodynamic therapy. *Photodiagn. Photodyn. Ther. 8*, 14−29.
(36) Wieczorek, S., Schwaar, T., Senge, M. O., and Börner, H. G. (2015) Specific Drug Formulation Additives: Revealing the Impact of Architecture and Block Length Ratio. *Biomacromolecules 16*, 3308−3312.
(37) Wieczorek, S., Dallmann, A., Kochovski, Z., and Börner, H. G. (2016) Advancing Drug Formulation Additives toward Precision Additives with Release Mediating Peptide Interlayer. *J. Am. Chem. Soc. 138*, 9349−9352.
(38) Wieczorek, S., Vigne, S., Masini, T., Ponader, D., Hartmann, L., Hirsch, A. K. H., and Börner, H. G. (2015) Combinatorial Screening for Specific Drug Solubilizers with Switchable Release Profiles. *Macromol. Biosci. 15*, 82−89.
(39) Sutton, J. M., Clarke, O. J., Fernandez, N., and Boyle, R. W. (2002) Porphyrin, chlorin, and bacteriochlorin isothiocyanates: Useful reagents for the synthesis of photoactive bioconjugatest. *Bioconjugate Chem. 13*, 249−263.
(40) Chen, Y. H., Li, G. L., and Pandey, R. K. (2004) Synthesis of bacteriochlorins and their potential utility in photodynamic therapy (PDT). *Curr. Org. Chem. 8*, 1105−1134.
(41) Nyman, E. S., and Hynninen, P. H. (2004) Research advances in the use of tetrapyrrolic photosensitizers for photodynamic therapy. *J. Photochem. Photobiol., B 73*, 1−28.
(42) Sternberg, E. D., Dolphin, D., and Bruckner, C. (1998) Porphyrin-based photosensitizers for use in photodynamic therapy. *Tetrahedron 54*, 4151−4202.
(43) Silva, E. F. F., Serpa, C., Dabrowski, J. M., Monteiro, C. J. P., Formosinho, S. J., Stochel, G., Urbanska, K., Simoes, S., Pereira, M. M., and Arnaut, L. G. (2010) Mechanisms of Singlet-Oxygen and Superoxide-Ion Generation by Porphyrins and Bacteriochlorins and their Implications in Photodynamic Therapy. *Chem. - Eur. J. 16*, 9273−9286.

DOI: 10.1021/acs.bioconjchem.6b00549
Bioconjugate Chem. 2017, 28, 760−767

(44) Benov, L. (2015) Photodynamic Therapy: Current Status and Future Directions. *Med. Princ. Pract. 24*, 14−28.
(45) Bonnett, R. (1999) Photodynamic therapy in historical perspective. *Rev. Contemp. Pharmaco. 10*, 1−17.
(46) Zabihi, F., Wieczorek, S., Dimde, M., Hedtrich, S., Börner, H. G., and Haag, R. (2016) Intradermal Drug Delivery by Nanogel-Peptide Conjugates; Specific and Efficient Transport of Temoporfin. *J. Controlled Release 242*, 35−41.
(47) Juskowiak, G. L., McGee, C. J., Greaves, J., and Van Vranken, D. L. (2008) Synthesis, Screening, and Sequencing of Cysteine-Rich One-Bead One-Compound Peptide Libraries. *J. Comb. Chem. 10*, 726−731.
(48) Pucelik, B., Arnaut, L. G., Stochel, G., and Dabrowski, J. M. (2016) Design of Pluronic-Based Formulation for Enhanced Redaporfin-Photodynamic Therapy against Pigmented Melanoma. *ACS Appl. Mater. Interfaces 8*, 22039−22055.
(49) Gerber, P. R., and Müller, K. (1995) MAB, a generally applicable molecular force field for structure modelling in medicinal chemistry. *J. Comput.-Aided Mol. Des. 9*, 251−268.
(50) Sadowski, J., Gasteiger, J., and Klebe, G. (1994) Comparison of Automatic Three-Dimensional Model Builders Using 639 X-ray Structures. *J. Chem. Inf. Model. 34*, 1000−1008.

DOI: 10.1021/acs.bioconjchem.6b00549
Bioconjugate Chem. 2017, 28, 760−767